New Mass-Spring System Integrating Elasticity Parameters in 2D

Vincent Baudet, Michael Beuve, Fabrice Jaillet, B. Shariat, Florence Zara

Research Report - LIRIS - UMR CNRS 5205 - February 2007.

V. Baudet · M. Beuve · F. Jaillet · B. Shariat · F. Zara

New Mass-Spring System Integrating Elasticity Parameters in 2D

Abstract Besides the finite element method, the mass-spring discrete modeling is widely used in computer graphics. This discrete model allows to perform very easily interactive deformations and to handle quite complex interactions with only a few equations. Thus, it is perfectly adapted to generate visually correct animations. However, a drawback of this simple formulation is the relative difficulty to control efficiently physically realistic behaviors. Indeed, none of the existing models has succeeded to deal satisfyingly with this. Moreover, we demonstrate that the mostly cited technique in the literature, proposed by Van Gelder, is far to be exact in most real cases and its interest is limited to some specific non realistic animations. Here, we propose a new general 2D formulation that reconstructs the geometrical model as an assembly of elementary "bricks". Each brick (or element) is then transformed into a mass-spring system, in which edges are springs connecting masses placed on the element vertices. The key point of our approach is the determination of the stiffness constant of each spring to reproduce the correct mechanical properties (Young's modulus, Poisson's ratio and shear modulus) of the reconstructed object. We validate our methodology with the help of some numerical experimentation of mechanics, like stretching, shearing and loading and then we evaluate the accuracy limits of our approach.

Keywords Physically based Modeling · Mass-Spring System · Mechanical Parameters

V. Baudet
LSIIT-IGG, UMR CNRS 7005, Illkirch, F-67412, France
Tel.: +33 3 90 24 45 57 - Fax: +33 3 90 24 45 55
E-mail: vincent.baudet@gmail.com

M. Beuve · F. Jaillet · B. Shariat · F. Zara
LIRIS-SAARA, UMR CNRS 5205, Université Lyon 1, Villeurbanne, F-69622, France
E-mail: {mbeuve,fjaillet,bshariat,fzara}@liris.cnrs.fr

1 Introduction

In order to simulate accurately deformations occurring in a volume, models based on continuous media mechanics are used with finite elements resolution methods. The models simulate accurately the mechanical behavior, but require a rigorous description of the boundary conditions, which is hardly compatible with any unpredictable interactions. Moreover, the dimensions of the applied strains and stresses must be well defined to choose either a small - with Cauchy's description - or a large deformation context - with St Venant Kirchoff's description. Indeed, the two contexts are accurate only on their domain of deformation.

In the literature, discrete models (like mass-spring systems) coming from computer-graphics animation are generally proposed to deal with the real time applications and to allow unpredictable interactions and large or small deformations. They are used in virtual reality environments where many unpredicted collisions with small or large deformations may occur. Medical or surgery simulators present another example of their possible applications. Nevertheless these models generally fail to represent accurately the behavior of real objects.

In this paper, we propose a new method that gathers the advantages of both approaches. Section 2 presents some previous work on mass-spring systems and particularly their parameterization. Section 3 describes Van Gelder's model, which incorporates spring parameters calculated from the elasticity parameters. We prove that this model cannot simulate correctly 2D deformations and in section 4, we propose an alternative model. Section 5 presents an evaluation through numerical experiments. Then, some results of the extension of our approach to 3D, are given. Finally, concluding remarks and perspectives are provided in section 6.

2 Related Work

Mass-spring systems have largely been used in the animation context because of their simple implementation and also because they can be applied to a large panel of deformations. They consist in describing a surface or a volume with a mesh in which the global mass is uniformly distributed over the mesh nodes. The elasticity is represented by springs at every edge. Newtons laws govern the dynamics of the model.

Mass-spring system have been used to model textiles [12,14,27], long animals such as snakes [18], or soft organic tissues, such as muscles, face or abdomen, with sometimes the possibility to simulate tissue cut [1,7,16, 17,20,21,26]. Moreover, these systems have been used to describe a wide range of different elastic behaviors such as anisotropy [4], heterogeneity [28], non linearity [5] and also incompressibility [24,25].

An important problem of these models is to choose an appropriate meshing that describes well the object and that does not contain any privileged direction for the strains propagation. Then, the springs elasticity must be rigorously defined to achieve the desired behavior. Despite this requirement, springs stiffness constants are generally empirically set [19].

Solutions based on simulated annealing algorithms or genetic algorithms [2,3,10,13] give access to spring stiffness constants. Usually they consist in applying random values to different springs constants and in comparing the obtained model with some mechanical experiments in which results are either well known analytically or can be obtained by finite element methods. The stiffness constant of the springs that induce the greatest error is corrected to minimize the discrepancies. However, the efficiency of this process depends on the number of springs and is based on numerous mechanical tests leading to quite expensive computation time. Moreover, the process should be repeated after any mesh alteration.

Instead of a try-and-error process, a formal solution to parameterize the springs should save computer resources. In this context, two approaches were explored. The Mass-Tensor approach [8,23] aims at simplifying finite element method theory by a discretization of the constitutive equations on each element. But, despite its interest, this approach requires pre-computations and the storage of an extensive amount of information for each mesh component (vertex, edge, face, element).

The second approach proposed by Van Gelder [29], referenced in [4,6,9,15,21,22,30], introduces mechanical parameters (Young's modulus and Poisson's ratio) in a simple mass-spring system. This approach combines the advantages of an accurate mechanical parameterization with a hyper-elastic model, enabling either small or large deformations. This model will be studied in the next section.

3 Van Gelder Model

This section is concerned with the mechanical description of 2D system. In 1998, Van Gelder [29] proposed a new formulation for triangular meshes, allowing to calculate spring stiffness constant according to elastic parameters of the object to simulate. Thus, in this model, the stiffness constant of a spring, with a rest length c, representing the common edge of two neighboring triangles of the mesh (T_1 and T_2) of surfaces $|T_i|$ and with edges a_i, b_i and c, $i \in \{1,2\}$, is given by:

$$k_c = \sum_{i=1}^{n} \frac{E}{1+\nu}\frac{|T_i|}{c^2} + \frac{E\,\nu}{1-\nu^2}\frac{a_i^2+b_i^2-c^2}{8\,|T_i|}, \tag{1}$$

with ν the Poisson's ratio and E the 2D Young's modulus of the simulated material (see Fig. 1).

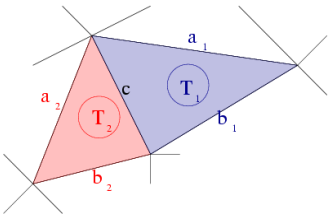

Fig. 1 Annotations used in the Van Gelder model.

Van Gelder's published experimentations are restricted to $\nu = 0$ to avoid negative value of k_c. To cope with the reality, we used Van Gelder's approach to simulate materials with $\nu \geq 0$. Firstly, we simulated the well-known traction test using a bar of dimensions $l_0 \times h_0$. For the sake of simplicity, experimentations were carried out on a square object ($l_0 = h_0$) meshed by four symmetrical Van Gelder (VG) triangles (see Fig. 2). The input Young's modulus is noted E_{VG} and input Poisson's ratio ν_{VG}. The spring stiffness constants were calculated according to equation (1).

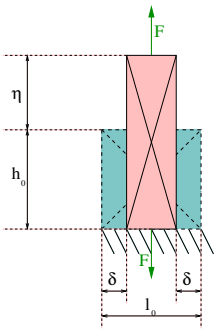

Fig. 2 The bar of dimension $l_0 \times h_0$ is elongated by a force $\mathbf{F}$, generating a stretch η and a compression of range 2δ at equilibrium.

Note that due to symmetry, we can distinguish only two kinds of spring stiffness constants: (i) k_e for the edges of the bar, (ii) k_d for its semi-diagonals. At one end, the bar is elongated by a force $\mathbf{F}$, generating a stretch η

and a thinning 2δ (Fig. 2). The other end is fixed in the elongation direction but let free in the lateral direction. With such boundary conditions, the elastic parameters of the bar are defined by [11]:

$$\nu = \frac{2\delta/l_0}{\eta/h_0}, \quad E = \frac{F/l_0}{\eta/h_0}. \tag{2}$$

To be consistent, the Van Gelder's model should give:

$$\nu_{VG} = \nu, \quad E_{VG} = E. \tag{3}$$

Poisson's ratio		**Young's modulus (Pa.m)**	
ν_{VG}	ν	E_{VG}	E
0.0	0.5	0	0
		1	0.75
		100	75.00
		1000	750.00
0.25	0.57	0	0
		1	0.63
		100	62.86
		1000	628.57
0.5	0.66	0	0
		1	0.56
		100	55.56
		1000	555.56

Table 1 Comparison tests between input Poisson's ratio ν_{VG}, input Young's modulus E_{VG} and theoretical values ν and E.

However, the simulations results presented in Table 1 show that this is not the case. Even when Poisson's ratio is set to zero, we note an error of 25% on the Young's modulus, although the authors claimed that their model was valid for this specific value, used for membranes.

To generalize this observation we proposed a demonstration in the framework of Lagrangian formulation. Thereby we had to:

1. Define the potential energies of springs according to their elongations (η and δ) and the potential energy of the applied forces.
2. Define the Lagrangian as the sum of the different static potential energies (note that kinetic energies are null).
3. Deduce the values of the deformations (η and δ) by the application of the Least Action Principle.
4. Calculate the actual value of the Young's modulus and the Poisson's ratio of the bar.

For the sake of simplicity the calculations were restricted to very small deformations to linear equations. It reads:

$$E = \frac{F/l_0}{\eta/h_0} = \frac{1}{2}\frac{E_{VG}(\nu_{VG}-3)}{\nu_{VG}^2 - \nu_{VG} - 2}, \; \nu = \frac{2\delta/l_0}{\eta/h_0} = \frac{1}{2-\nu_{VG}}.$$

Again the relations $E = E_{VG}$ and $\nu = \nu_{VG}$ are not satisfied. Moreover, we notice that the Young's modulus depends on the Poisson's ratio, although the two characteristics should be totally independent in linear, isotropic and homogeneous materials [11]. Thereby, this model can difficultly be used to control realistically the elastic parameters.

In the next section, we will present a new 2D model that integrates more accuracy into the above-mentioned elastic parameters of a mass-spring system.

4 Our 2D Model

In our mass-spring approach, each element of the mesh can be characterized by a Young's modulus and a Poisson's ratio. At rest, the elements are identical rectangles with dimensions $l_0 \times h_0$. To integrate the role of the Poisson's ratio, we add two diagonal springs. Since we restrict this study to homogeneous and isotropic materials, the mechanical properties are the same for all the elements. It also implies the same stiffness constant for both the diagonal springs (k_d) and an equal stiffness constant for springs laying on two parallel edges (k_{l_0} and k_{h_0}) (see Fig. 3).

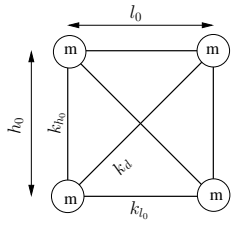

Fig. 3 2D element composition: rectangle composed of 4 masses m and 3 pairs of springs k_{l_0}, k_{h_0} and k_d.

Our aim is to deduce spring stiffness constants from mechanical characteristics. In addition to the Young's modulus and the Poisson's ratio (eq. (2)), the model should simulate correctly the reaction of the object to shearing strains (correct shear modulus) (see Fig. 4).

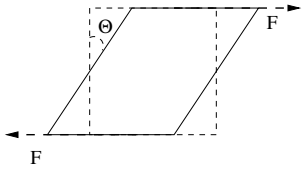

Fig. 4 Experimentation to measure the 2D shear modulus: a rectangular element is subject to 2 opposed forces, generating a deviation θ.

In 2D, the shearing modulus is measured by applying two opposed forces F resulting in shear stress F/l (with l the length of the edge) on two opposite edges of a rectangular sample of the material. The material response to shearing stress is a lateral deviation with an angle θ (see Fig. 4). Shear modulus is defined as:

$$G = \frac{tan\,(\theta) \times F}{l} \simeq \frac{\theta \times F}{l} \text{ when } \theta \to 0.$$

For linear elastic, isotropic and homogeneous materials, this coefficient is linked to the Young's modulus and the Poisson's ratio by $E = 2G\,(1+\nu)$.

To determinate the spring coefficients, we followed the method employed to demonstrate the inconsistence of Van Gelder 's model, except that all the springs coefficients are considered unknown:

1. For each experiment, we define the Lagrangian (sum of potential energies).
2. We apply the principle of least action to get the Newton equations.
3. We apply the definition of the measured mechanical characteristics to build a set of equations linking the spring coefficients to the mechanical characteristics.
4. We solve the whole system.

Before solving the system and considering the shear experiment, one notes that only the diagonal springs are stressed. Thus, the Lagrangian equation defining this characteristic depends only on k_d. This means that the diagonal springs are totally correlated to the shear modulus and that their stiffness constant can be calculated independently of the two other coefficients with the following relation:

$$k_d = \frac{E\left(l_0^2 + h_0^2\right)}{4 l_0 h_0 \left(1+\nu\right)}.$$

Note that, for a square mesh element, we obtain:

$$k_d = \frac{E}{2\left(1+\nu\right)} = G.$$

Consequently, the number of unknowns are now 2: k_{l_0} and k_{h_0}. To solve the system, the number of unknowns has to be equal to the number of equations (constraints). Two equations result from each elongation experiment. Thus we obtain four equations, if we include both lateral and longitudinal directions. This over-constrained system admits one solution for $\nu = 1/3$. This is not satisfactory because we wish to simulate the behavior of any real material. One needs to add two degrees of freedom.

We note that the Poisson's ratio defines the thinning at a given elongation, *i. e.* it determines the forces orthogonal to the elongation direction. By modifying the compression forces, we will be able to act on the Poisson's ratio ν. Thus, we introduced for each direction a new variable that defines this orthogonal force. The force orthogonal to h_0 (resp. l_0) is noted $F_{\perp h_0}$(resp. $F_{\perp l_0}$) (see Fig. 5). Note that this kind of correction is equivalent to the reciprocity principle used in finite elements methods [11]. The addition of these 2 new variables leads to a system of 4 equations with 4 unknowns.

The solution of the new system is:

$$k_i = \frac{E\left(j^2\left(3\,\nu+2\right) - i^2\right)}{4\;l_0\;h_0\left(1+\nu\right)}, \quad F_{\perp i} = \frac{j\;F_i\left(1-\nu\right)}{8i},$$

with $(i,j) \in \{l_0, h_0\}^2$ with $i \neq j$. In this definition, k_i must be positive implying the following constraint on the angle noted α, between the diagonal and one of the edges of the rectangle (see Fig. 5):

$$\arctan\left(1/\sqrt{3\nu+2}\right) < \alpha < \arctan\left(\sqrt{3\nu+2}\right).$$

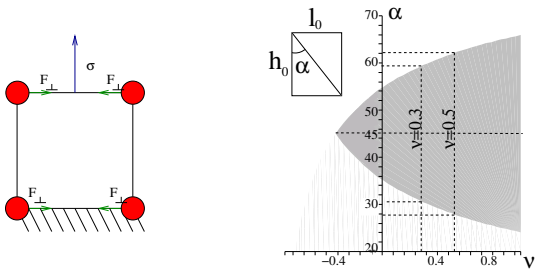

Fig. 5 (Left) Correction forces. (Right) The geometry of the model is restricted according to the Poisson's ratio: for $\nu = 0.3$, the angle α must satisfy $30 < \alpha < 60$.

Because of symmetry, the 6 springs of each element are only defined by three spring coefficients and the elongation/compression correction forces.

To simulate the object, which is built with an assembly of the elements defined above, we have first to compute all the forces applied to each element. These forces can be (i) internal, including forces due to springs and correction forces, or (ii) external, like gravity or forces due to the reaction to neighboring mesh elements. Note that, to compute the correction forces applied on an edge, we have to compute the elongation force, which is the sum of all the external forces applied to the considering edge projected on its orthogonal axis. Then, simulating the deformation of a mesh element due to external constraints consists in:

1. Computing the forces applied to each element.
2. Calculating accelerations and velocities, according to an integration scheme (explicit or implicit Euler, Verlet, etc.).
3. Displacing each node consequently.

The next section will describe numerical experimentations to verify that the object has the same mechanical characteristics as the elements composing it. Then, we will evaluate the accuracy limits of our model.

5 Evaluation of the 2D Model

In the previous section, we proposed a model that provides the stiffness constants and the amplitude of the thinning forces. This derivation was obtained in the limits of very small deformations (Taylor expansion to first order). We propose now to qualify the mechanical properties of the meshed systems even for important deformations (up to 20%).

Tensile stress limits

Performing elongation test allowed us to point out when our model deviates from the expected behavior. In each experiment, we applied quasi-static tensile stress steps up to 20% of the beam length. Each experiment was done for an imposed 2D Young's modulus E, with values varying from 0.01 Pa.m to 1 Pa.m, and an imposed Poisson's ratio ν, varying from 0.1 to 0.5. These tests have been realized on rectangular mesh elements with different shape ratios. In each case, the mesh angle restriction, as defined in Fig. 5, has been respected. The simulated output quantities are compared to the input parameters.

First, let consider the case of a square element. We observed that Young's modulus (see Fig. 6) and Poisson's ratio (see Fig. 7 and 8) of our model tend to drift when the deformation increases. Nevertheless, these values are really satisfying. As illustrated in Fig. 6, error on Young's modulus exceeds 5% only for deformations higher than 11%.

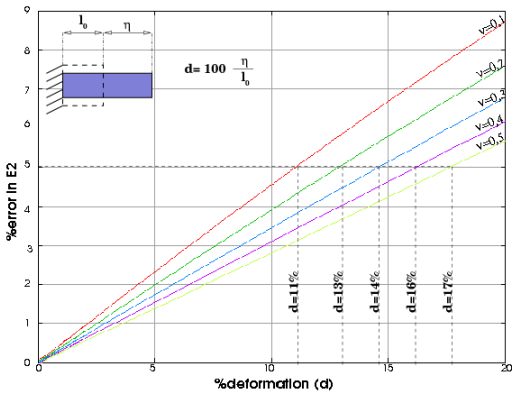

Fig. 6 2D Young's modulus errors for a square mesh element in quasi-static tensile stress.

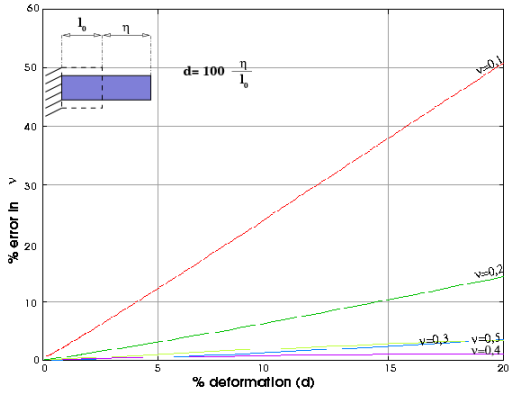

Fig. 7 Poisson's ratio errors (absolute value) for a square element in tensile stress.

Besides, we notice that this error increases conversely with the imposed Poisson's ratio: for a 10% deformation, the error on Young's modulus is 3.5% for $\nu = 0.3$, 3.1% for $\nu = 0.4$, and 2.8% for $\nu = 0.5$. For the Poisson's ratio, the error does not exceed 5% for $\nu \in [0.3; 0.5]$ and a deformation lower than 20% (see Fig. 8). In addition, if we repeat these experiments with different Young's moduli, we find exactly identical curves whatever the imposed value of E is. This is not surprising since the spring stiffness constants and the thinning forces are proportional to the input parameter E.

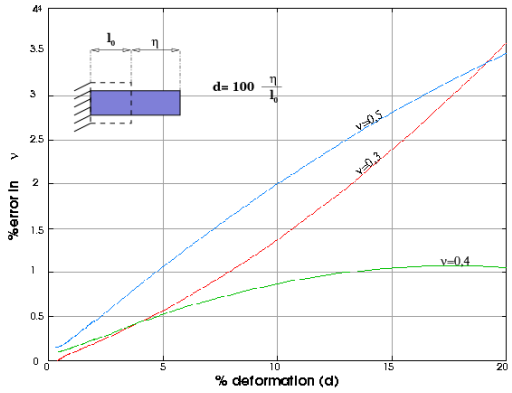

Fig. 8 Magnification for ν from 0.3 to 0.5.

We note beside that the profile of the ν error changes at $\nu = 0.3$. This is due to the fact that in this case, there is no need for any corrective Lagrangian force. Indeed, thinning is overestimated for $\nu < 0.3$ and underestimated for $\nu > 0.3$.

If one reiterates these experiments for rectangular elements defined such that the stiffness coefficients are positive (see Fig. 5), we note that the Young's modulus error increases with the angle α between the edge and the diagonal. In other words, when stretching along the smallest side of a rectangle, the error is very small. On the other hand, by reproducing the tensile test, on the largest side, the error will be larger. However, in the worst cases, errors are lower than 5% for $\nu \in [0.3; 0.5]$ and deformations lower than 10%.

The same observations can be derived for Poisson's ratio for which the error is lower than 5% in the same conditions.

One of the problems linked to deformations larger than 10% is the variation of the angle α which can result in negative stiffness values (see Fig 5). Therefore, to achieve deformation greater than 10% with better precision, square elements possessing an initial value of 45 degrees for α, give a more important safety margin to obtain positive stiffness constants. To end we verified that the error is the same whatever the number of elements that compose the object is.

Limits in shearing

Now, we replace the tensile stress by a shear stress (as illustrated in Fig. 4), and measure the errors for different shear angles. Figure 9 presents the results for a square mesh element.

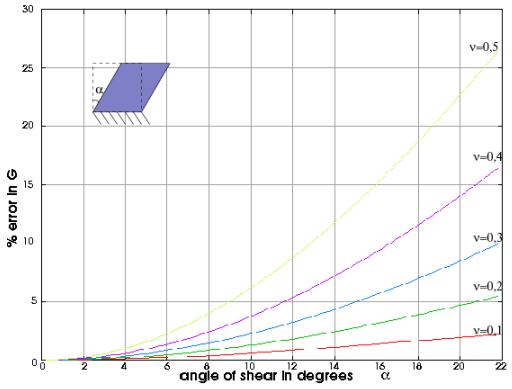

Fig. 9 Measured error on shearing in a square according to angle and Poisson's ratio.

We can remark that the relative error on G does not depend on E, as expected. It increases with the imposed ν but remains smaller than 5% for a shearing angle inferior to 9°. The worst case is for $\nu = 0.5$.

The extension of the simulations to rectangular element gives the same trends. When angle to the diagonal is $\alpha = 30°$, the error is inferior to 0.1% for an 8° shearing. However, if we apply the shearing in the other direction with $\alpha = 60°$, the error attains 5%.

Finally, it remains to validate the shearing on a composition of mesh elements. For this, we built a 100×300 mm beam by assembling elements characterized by $E = 1$ Pa.m and $\nu = 0.3$. Then we stressed the assembly by applying a force of 2000 N.

To evaluate the behavior of our model, we used as reference a linear elastic Finite Element Model (FEM). The results of our simulations are superimposed to the FEM reference (see Fig. 10). Within the theoretical framework of our model, *i. e.* small deformations, the agreement is very satisfactory.

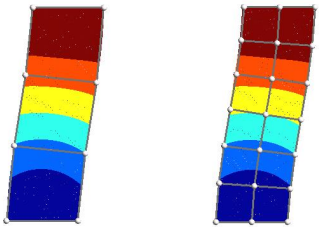

Fig. 10 Shearing experience: superimposition of the results of our wired model with the color gradation FEM reference solution: (Left) 1×3 elements composition; (Right) 2×6 elements composition.

Limits in deflection

The deflection experience (construction or structural element bending under a load) is recommended to validate mechanical models. It constitutes in particular a relevant test to evaluate (a) the correct mass repartition, and (b) the good behavior in case of large deformations (because of large rotation displacement, especially close to the fixation area).

This test consists in observing the gravity-induced deformation of a beam anchored at one end to a support. At equilibrium, the top of the beam is under tension while the bottom is under compression, leaving the middle relatively stress-free with shear stress above the support. The length of the zero stress line will remain unchanged (see Fig. 11).

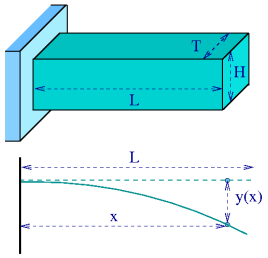

Fig. 11 Cantilever submitted to gravity, expression of the neutral axis deviation.

If the Poisson's ratio is null, the deviation of the neutral axis is given by (in 3D):

$$y\,(x) = \frac{\rho g}{24\ E_3 I}\left(6\ L^2 x^2 - 4\ L\ x^3 + x^4\right), \tag{4}$$

for the rectangular beam of inertia moment $I = TH^3/12$, with linear density $\rho = M/L$, and the 3D Young's modulus $E_3 = E/T$.

In 2D, we notice that results depend on the mesh resolution (as for any other numerical methods), however the fiber axis profile is similar to the equation (4).

Fig. 12 shows some results for a cantilever beam of dimensions 300×100 mm, with Young's modulus equal to 1 Pa.m, Poisson's ratio to 0.3 and total mass to 0.5 Kg.

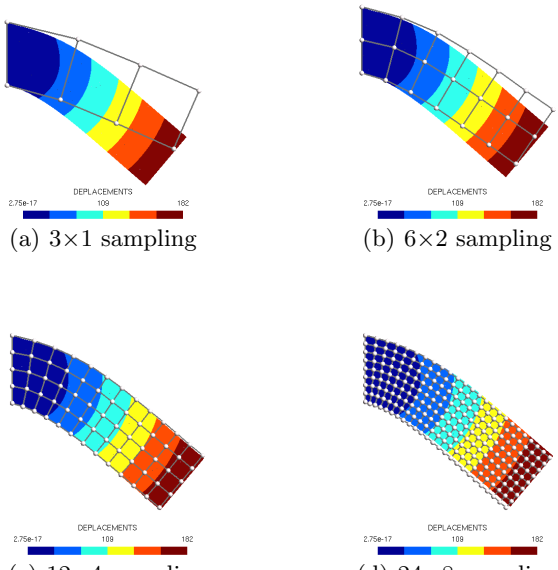

(a) 3×1 sampling (b) 6×2 sampling

(c) 12×4 sampling (d) 24×8 sampling

Fig. 12 Deflection experiment: the reference FEM solution (in color gradation) with superimposition of various simulations performed for different mesh resolutions).

Experiment on non symmetric object

Now, we test our model on an object in which the constraints are not applied along a symmetrical axis. Fig. 13 presents this object fixed at its base. We apply a constant force to the edges that are orthogonal to the base. Fig. 13 shows our results superimposed to the FEM solution.

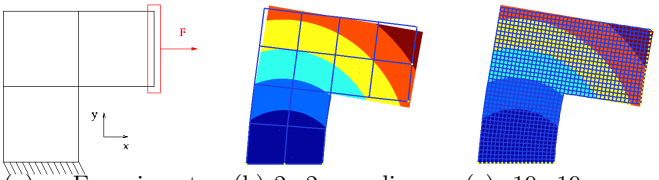

(a) Experiment description (b) 2×2 sampling (c) 19×19 sampling

Fig. 13 Experiment on a non symmetric object: superimposition of results obtained with FEM method (in color gradation) with our results performed for different mesh resolutions.

Table 2 resumes mean errors and standard deviation between the FEM gold standard and various displacements. These results are obtained at different meshing resolution of the above model. It is worth noticing that our model behaves as expected: better mesh resolutions lead to better results.

Resolution	Mean Errors in displ. (mm)	Standard Deviation in displ. (mm)
1×1	236,63	62,47
2×2	83,78	14,08
3×3	47,54	6,35
4×4	29,17	3,52
5×5	23,57	2,39
9×9	17,41	1,04
19×19	14,36	0,39

Table 2 Comparison of displacement errors of our method with the FEM reference.

Extension to 3D

In our recent works, the same 2D technique has been used for the extension of our model to 3D. We obtained very good preliminary results, comparable to 2D cases. Our actual 3D model is based on cubic elementary meshes including the inner diagonals. The stiffness parameters are calculated with respect to the Young's modulus, Poisson's ratio, shearing modulus and also compressibility modulus. For deformations less than 15%, the results are quite conform to the reality, with an error less than 5% for each mechanical characteristics. Several qualitative verification of our results have been carried out by their comparison with FEM reference solution (see Fig. 14).

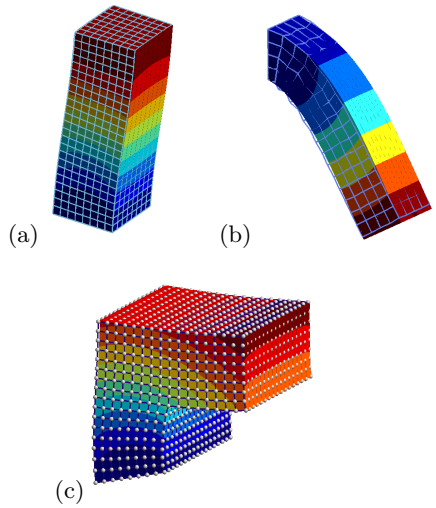

(a) (b) (c)

Fig. 14 Superimposition of results obtained with FEM method (in color) with our model (in wire mesh) of (a) a shearing experiment, (b) a deflection experiment, (c) a test combining shearing and elongation on an object with no symmetrical shape.

6 Conclusion and Future Work

Looking for a method to obtain a fast and accurate model that combines large and small deformations, we studied the mass-spring system model developed by Van Gelder. Even if this approach, allowing to calculate spring stiffness constants according to mechanical parameters, seemed very attractive, we proved that this model, developed for small deformations and applied to linear elastic, isotropic and homogeneous material was not totally correct. Then, we proposed a new model within a Lagrangian framework.

The object is first meshed with rectangular mass-spring mesh elements, with two diagonals. We demonstrated that for this kind of mesh elements, a simple mass-spring system couldnt accurately simulate the material behavior with any Poisson's ratio. Consequently, we proposed to add correction forces orthogonal to the elongation forces in order to compensate the error on Poisson's ratio. By construction, our model is well characterized by the Young's modulus and Poisson's ratio for small deformations. Limits of our model have been given by comparing our results with those obtained by a finite element method as reference for preciseness.

We exhibited that our model can support larger deformations with square mesh elements. Indeed for any value of Young's modulus and Poisson's ratio, it allows to simulate within acceptable error margins stretching up to 10% and shearing $< 9°$.

Besides, we verified the correct behavior of an assembly of mesh elements. This shows that contrary to FEMs, we can expect to use a mass-spring system to simulate either large or small deformations.

We extended our model to 3D by using cubic mesh elements. The obtained results have been very successful.

In the future, we are looking to apply the same technique to other geometries, for example to triangle or any quadrangle in 2D, or parallelepiped in 3D, to increase the possibilities and to offer more tools for simulating complex shapes.

Moreover, it may be interesting to investigate how and when to update the springs coefficients and correction forces to improve the results in case of large deformations. Another track to reduce errors is to adapt locally the resolution of the mesh elements. For example, we can modify the resolution in the vicinity of highly-deformed zones, reducing large rotations of elements undergoing heavy load.

References

1. Aubel, A., Thalmann, D.: Realistic deformation of human body shapes. In: Computer Animation and Simulation '00, pp. 125–135 (2000). URL citeseer.ist.psu.edu/aubel00realistic.html
2. Bianchi, G., Solenthaler, B., Székely, G., Harders, M.: Mesh topology for mass-spring models. In: Springer-Verlag (ed.) MICCAI 2003, pp. 50–58. Berlin (2003)
3. Bianchi, G., Solenthaler, B., Székely, G., Harders, M.: Simultaneous topology and stiffness identification for mass-spring models based on FEM reference deformations. In: Springer-Verlag (ed.) MICCAI 2004, pp. 293–301. Berlin (2004)
4. Bourguignon, D.: Interactive animation and modeling by drawing - pedagogical applications in medicine. Ph.D. thesis, Institut National Polytechnique de Grenoble (2003)
5. Boux de Casson, F.: Simulation dynamique de corps biologiques et changements de topologie interactifs. Ph.D. thesis, Université de Savoie (2000)
6. Bruyns, C., Ottensmeyer, M.: Measurements of soft-tissue mechanical properties to support development of a physically based virtual anima model. In: MICCAI 2002, pp. 282–289 (2002)
7. Chadwick, J., Haumann, D., Parent, R.: Layered construction for deformation animated characters. Computer Graphics **23**(3), 243,252 (1989)
8. Cotin, S., Delingette, H., Ayache, N.: Efficient linear elastic models of soft tissues for real-time surgery simulation. Proceedings of the Medecine Meets Virtual Reality (MMVR 7) **62**, 100–101 (1999)
9. Debunne, G.: Animation multirésolution d'objets déformables en temps réel, application la simulation chirurgicale. Ph.D. thesis, Institut National Polytechnique de Grenoble (2000)
10. Deussen, O., Kobbelt, L., Tucke, P.: Using simulated annealing to obtain good nodal approximations of deformable objects. In: Springer-Verlag (ed.) Proceedings of the Sixth Eurographics Workshop on Animation and Simulation, pp. 30–43. Berlin (1995)
11. Feynman, R.: The Feynman Lectures on Physics, vol. 2. Addison Wesley (1964). Chapter 38
12. Keckeisen, M., Etzmu, O., Hauth, M.: Physical models and numerical solvers for cloth animations. In: Simulation of Clothes for Real-time Applications, vol. Tutorial 1, pp. 17–34. INRIA and the Eurographics Association (2004)
13. Louchet, J., Provot, X., Crochemore, D.: Evolutionary identification of cloth animation models. In: Springer-Verlag (ed.) Proceedings of the Sixth Eurographics Workshop on Animation and Simulation, pp. 44–54. Berlin (1995)
14. Luciani, A., Jimenez, S., Florens, J.L., Cadoz, C., Raoult, O.: Computational physics : A modeler-simulator for animated physical objects. In: Proceedings of Eurographics 91, pp. 425,436. Eurographics, Amsterdam (1991)
15. Maciel, A., Boulic, R., Thalmann, D.: Deformable tissue parameterized by properties of real biological tissue. citeseer.nj.nec.com/574309.html (2002)
16. Meier, U., López, O., Monserrat, C., Juan, M.C., Alcañiz, M.: Real-time deformable models for surgery simulation : a survey. Computer Methods and Programs in Biomedicine **77**(3), 183–197 (2005)
17. Meseure, P., Chaillou, C.: Deformable body simulation with adaptative subdivision and cuttings. In: 5th Int. Conf. in Central Europe on Comp. Graphics and Visualisation WSCG'97, pp. 361–370 (1997)
18. Miller, G.: The motion dynamics of snakes and worms. Computer Graphics **22**(4), 168,178 (1988)
19. Nealen, A., M´uller, M., Keiser, R., Boxerman, E., Carlson, M.: Physically based deformable model in computer graphics. Eurographics (2005). State of the Art report
20. Nedel, L.P., Thalmann, D.: Real-time muscles deformations using mass-spring systems. Computer Graphics International pp. 156–165 (1998)
21. Paloc, C.: Adaptative deformable model (allowing topological modifications) for surgical simulation. Ph.D. thesis, University of London (2003)
22. Picinbono, G.: Modèles géométriques et physiques pour la simulation d'interventions chirurgicales. Ph.D. thesis, Université de Nice Sophia-Antipolis (2001). Http://www.inria.fr/rrrt/tu-0669.html
23. Picinbono, G., Delingette, H., Ayache, N.: Non-linear anisotropic elasticity for real-time surgery simulation. Graphical Model (2003)
24. Platt, J., Barr, A.: Constraint methods for flexible models. Computer Graphics **22**(4), 279–288 (1988)
25. Promayon, E.: Modélisation et simulation de la respiration. Ph.D. thesis, Université Joseph Fourier, Grenoble (1997)
26. Promayon, E., Baconnier, P., Puech, C.: Physically based deformation constrained in displacements and volume. In: Proceedings of Eurographics'96. BlackWell Publishers, Oxford (1996)
27. Provot, X.: Deformation constraints in a mass-spring model to describe rigid cloth behavior. In: Proceedings of Graphics Interface 95, pp. 147,154. Canadian Human-Computer Communications Society, Toronto (1995)
28. Terzopoulos, D., Waters, K.: Physically-based facial modelling, analysis, and animation. The Journal of Visualization and Computer Animation **1**, 73–80 (1990)
29. Van Gelder, A.: Approximate simulation of elastic membranes by triangulated spring meshes. Journal of Graphics Tools **3**(2), 21–42 (1998)
30. Wilhelms, J., Van Gelder, A.: Anatomically based modelling. In: Computer Graphics (SIGGRAPH'97 Proceedings), pp. 173–180 (1997)